Inferring Multiple Tissue Properties from Magnetic Resonance Fingerprinting Images

Naren Nallapareddy, Soumya Ray
Case Western Reserve University
Department of Computer and Data Sciences
10900 Euclid Avenue,
Cleveland, OH 44106
nxn151@case.edu, sray@case.edu

Abstract

Magnetic Resonance Imaging (MRI) is a non-invasive imaging modality that is a cornerstone of diagnostic radiology. Clinical MRI scans capture a single image to highlight a single tissue property. The intensity difference between different regions of this image shows disease states that a radiologist can interpret. Magnetic Resonance Fingerprinting (MRF) is a recently proposed novel MRI technique. MRF allows the capture of multiple MR images in a single scan. This enables clinicians to analyze multiple tissue properties, potentially increasing the sensitivity of diagnosis and also allowing for the diagnosis of novel diseases. However, it is more challenging to analyze MRF images, because MRF produces much larger and noisier data than MRI. In this paper, we show how AI techniques can help solve this problem. Using a hybrid search strategy combining simulated annealing with pattern search, we show it is possible to tractably reconstruct multiple tissue properties from a single MRF image. This is a key step towards the deployment of MRF for radiological diagnosis.

Introduction

Magnetic Resonance Imaging (MRI) is an indispensable clinical tool for diagnosing and tracking several disease states noninvasively (Larsson et al. 1989; Kim et al. 2000; Jack et al. 2008). Radio frequency (RF) transmitter coils inside the scanner excite protons by disrupting tfrheir alignment with a strong magnetic field (Brown et al. 2014). Over time, these excited protons return to their initial state via relaxation processes that emit RF radiation that is captured using receiver coils. From the relaxation processes, we can capture quantitative data characteristic of the tissue. The longitudinal relaxation time **T1** (milliseconds) is a measure of time elapsed by excited protons to align back to the strong magnetic field. The transverse relaxation time **T2** ((milliseconds) is the time taken by protons spinning perpendicular to the main magnetic field to go out of phase with each other. Besides T1 and T2, MRI can also capture secondary properties, such as proton density and proton diffusion. We collectively refer to these as *tissue properties* (Ma et al. 2013).

In an MRI scan, the signal at each pixel in an image captures the frequency and phase information of protons. We can then construct an intensity image by applying a Fourier transform to the captured signal. This transformed intensity image does not in itself represent the values of tissue properties. Instead, this intensity image is used to identify regions of increased signal (hyperintense) or decreased signal (hypointense) compared to the normal (tissue lacking observable abnormalities). In the MR literature, these images are referred as "weighted" images to signify that a single tissue property of interest dominates the image. For example, Figure 1 shows a T1-weighted (**T1w**) image of the brain of a patient suffering from brain hemorrhaging (Ginat and Meyers 2012). The hyperintense blob in the image represents the extent and size of abnormality, which is interpreted by a clinician to make diagnostic decisions.

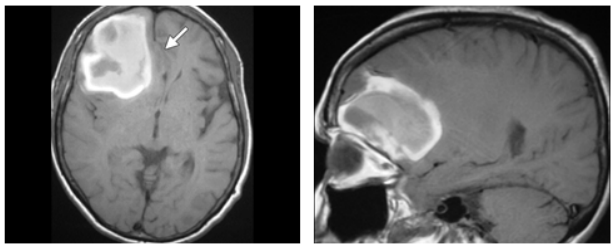

Figure 1: Image of a patient with brain haemorrhage as captured by a T1w scan in axial and sagittal planes. The large hyperintense blob indicates area affected by haemorrhaging (Ginat and Meyers 2012).

Individual clinical T1w and T2w MRI images are *qualitative* because they can change across scans. This is because the precise image depends on several factors, such as coil sensitivities, system imperfections and environmental variations. To obtain a reliable quantitative tissue property that is invariant to such factors, multiple sequential MR scans must be made for a tissue property. Then, the data for each pixel in each sequence of images is fit to a known behavioral curve for the chosen tissue property. This allows inferring the value of the tissue property for that pixel. This procedure is shown schematically in Figure 2. However, this process is expensive and time consuming because multiple scans must be made for each tissue property of interest. This limits radiologists from performing quantitative scans in clinical settings, or from using multiple tissue properties in diagnosis.

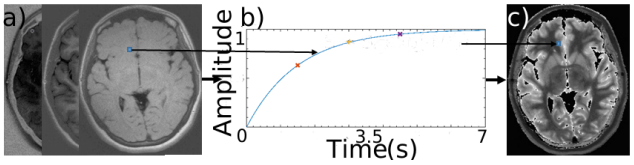

Figure 2: Traditional tissue property mapping pipeline. Here, several images (a) are generated that are dominated by a single tissue property, for example T1. Each pixel along the time axis is fit to an exponential curve. This allows inferring the values of T1 (Yao et al. 2018).

To address some of these drawbacks, a novel technique called Magnetic Resonance Fingerprinting (MRF) (Ma et al. 2013) has recently been introduced. MRF, described in detail in the next section, is a novel MRI framework that allows acquisition of multiple tissue property images in a *single* MR scan. Multiple tissue property images from a single scan decreases costs and discomfort faced by patients and can increase sensitivity in diagnosis. Access to multiple tissue properties may also allow for the use of MRF in novel diagnostic procedures as yet unknown. However, reconstructing tissue properties from MRF images is an algorithmic challenge. MRF produces noisy images for which there are no known mathematical models that can generate tissue property maps. Therefore, the traditional approach of fitting a curve to recover the tissue property cannot be applied. Instead, the state of the art is to use a template dictionary matching approach for reconstructing tissue properties (described in more detail below). This strategy, although robust (Jiang et al. 2017) does not scale well as the number of tissue properties increases. This is because both time and space requirements of this procedure are exponential in the number of tissue properties. Thus, a different approach is required. Our key insight is to observe that stochastic local search techniques in AI have been successfully used in many previous applications involving high dimensional parameter estimation. Thus we propose an approach based on this idea to interpret MRF images in a tractable manner. This is a key step toward the clinical deployment of MRF.

In the following section, we first explain how MRF acquires scans. Then we introduce our hybrid stochastic search approach to recover multiple tissue properties from a single MRF scan. We show empirically that our approach is comparable to template dictionary matching for recovering two tissue properties (Ma et al. 2013). We then show that the approach can estimate six tissue properties, which is impossible with state of the art methods. Finally we discuss remaining issues and the path to deployment of this approach.

Magnetic Resonance Fingerprinting

There are some basic similarities and fundamental differences between MRI signal acquisition and MRF signal acquisition. During the acquisition step in MRI, a pre-defined sequence of RF pulses on the RF coil in the scanner is executed. This is referred to in MR literature as a pulse sequence (Bernstein, King, and Zhou 2004). A set of pulse sequence parameters controls the amplitude, phase and delays in a fundamental period of the pulse sequence. Designing the pulse sequence parameters allows us to collect MR signal in predictable ways to increase the sensitivity of the captured signal to a single tissue property. For instance, in T1w imaging, a pulse sequence is played that can capture different points on the exponential decay curve of T1, shown in Figure 2. In MRI, there is a time delay between sampling of subsequent points on the exponential curve. This delay allows the protons to recover back to their original position. This delay is unavoidable during a conventional MRI. In MRF, we avoid this "dead time" by playing the pulse sequence with no delay, choosing the sequence in a way so that each pulse produces a different excitation in the underlying Fourier space. Different pulses can be sensitive to different tissue properties. This is one of the primary strengths of MRF; however, it implies that we are not sampling the exponential curve but a more complex signal trajectory. Further, the pulse sequence parameters at each fundamental period allow sampling of the frequencies and phases of the underlying Fourier space. In MRI, the Fourier space is sampled at a rate that is at or above the Nyquist rate. To decrease the time required to scan, in MRF, we sample a fraction of the Fourier space (usually at 1/24th of the Nyquist rate). The pattern in which we scan the image is an active research area (Körzdörfer et al. 2019). This decreases time to capture a single image, but increases the noise in the image that is captured at the scanner (Figure 3a). If we assume each image is of size $R \times R$, we capture T images for each pulse in the pulse sequence. The time taken to capture these T images is equivalent to time taken to capture three to five images captured during a conventional MRI scan. However, because of the way MRF pulse sequences are designed, this allows recovery of multiple tissue properties from a single scan that takes time comparable to a conventional MRI scan.

Tissue Parameter Recovery using Explicit Dictionary

In standard MRI, a known mathematical model is used to estimate the tissue property. For example, in T1 mapping, we fit a parametric exponential curve to the captured samples to recover the tissue property value (Figure 2). In MRF, each tissue parameter does not follow a known closed form curve. To solve this problem, (Ma et al. 2013) propose an explicit template dictionary based approach. The underlying idea is to *simulate* all known signal trajectories given by tissue parameter values. NMR Bloch equations (Bloch 1946) are differential equations that characterize precession of protons under the influence RF signal amplitude and phase. This allows simulating proton precession at δ time step (usually 1ms). In such Monte Carlo simulations, we allow multiple protons to precess and relax for each δ time step in a pulse sequence. The generated signal from the simulation is collected for each set of tissue property values to generate a template dictionary (Figure 3c). Next, we match the captured MRF signal trajectories (Figure 3b) with the template dictionary to retrieve the tissue property values. The match is performed by taking an inner product between the observed signal trajectory and each element of the dictionary. The dot

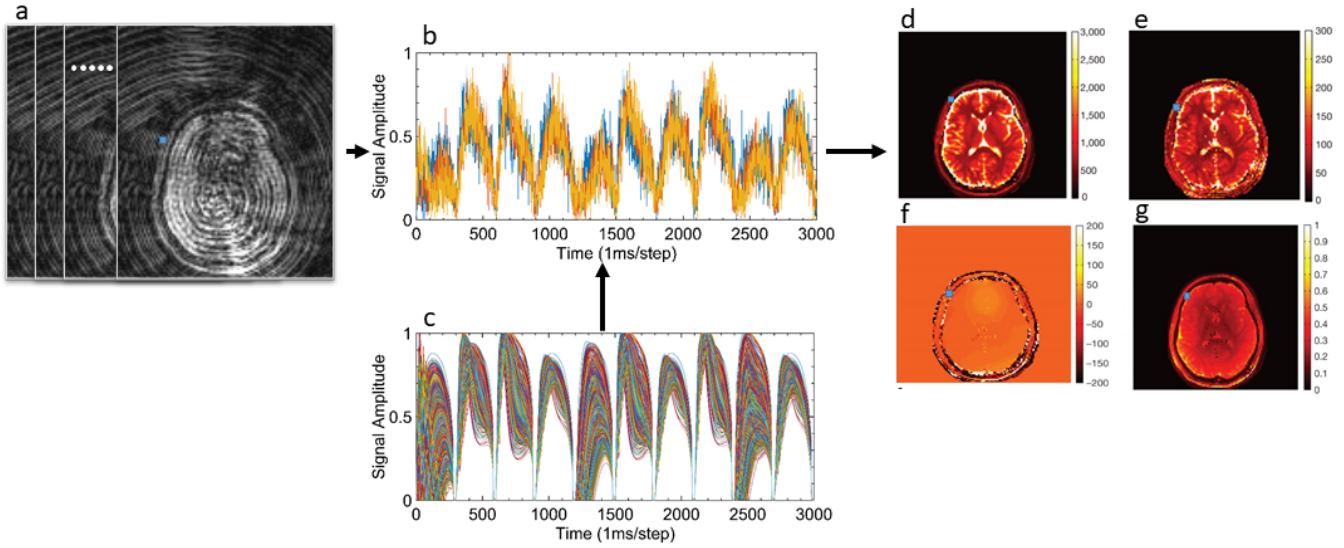

Figure 3: MRF tissue property mapping pipeline. Multiple noisy images (a) are captured at the scanner. Individual signals for each pixel (b) are compared with an explicit dictionary (c) to recover the tissue properties generating the signals. The generated maps represent tissue properties such as T1 (d), T2 (e), B1 mapping (f) and proton density (g) respectively (Ma et al. 2013).

product is a measure of the similarity of the two trajectories. The parameter yielding the highest dot product (most similar known trajectory) is selected as the tissue parameter. This process is repeated for each pixel in the input.

The original MRF paper describes reconstruction of two tissue properties, T1 and T2. Several authors have extended dictionary based matching to three or four tissue properties (Deshmane et al. 2019; Wang et al. 2019). While primary focus has been in increasing the speed of reconstruction, most of these methods (Cauley et al. 2015; Yang et al. 2018; McGivney et al. 2014) still depend on dictionary generation for tissue property recovery. Generating a large dictionary with millions of entries is slow and takes several gigabytes of memory during runtime. For example, we need to generate $196,000$ elements to get a precision of about $1-2\%$ in three tissue properties (Cauley et al. 2015). It takes 2 hours on an AMD based octa-core CPU and uses 0.8GB of memory during runtime to generate the dictionary. This *may* be tolerable for three tissue properties. With an increase in number of tissue properties, however, the dictionary grows exponentially large and tissue property recovery using such an explicit matching technique becomes infeasible.

Hybrid Search for Recovering Multiple Tissue Properties from MRF Images

In our work, we use the pulse sequence used in prior work (Hamilton, Griswold, and Seiberlich 2015) to generate *six* tissue properties that authors call MRF with exchange (MRF-X). The six tissue properties represent characteristics of two tissue environments that have an exchange of protons with each other. Each compartment is an independent tissue environment. For example, if a single pixel includes white matter region in brain, it has two independent environments, myelin (fat environment), and axon (non-fat environment). We want to estimate the tissue properties T1 and T2 for each separate environment, rate of exchange of protons between the environments (τ) and fractional volume occupied by the environments (ρ). To simplify notation, we will call T1 estimated in one of the environments as T1a (fast relaxation) and the other environment as T1b (slow relaxation). But we would like to do this *without* an explicit dictionary. Our key observation is that this is an optimization problem, and local search, in particular stochastic local search techniques in AI have been very successful at solving large optimization problems in prior work. So we propose a stochastic hybrid search method to provide a tractable alternative to dictionary matching for tissue parameter recovery in the 6D case.

Let us define each pixel in an MRF-X image sequence of size $R \times R \times T$ as X_{rst} where $(r, s, t) \in R \times R \times T$ are the row, column and time-step index of the image sequence. Each $1 \times 1 \times T$ vector in time is a function of p tissue property values. So, the input to the search technique is a $(R \times R) \times T$ image sequence and the output is $(R \times R) \times p$ tissue property maps. In our work we generate $p = 6$ tissue property maps consisting of tissue properties $T1a$, $T2a$, $T1b$, $T2b$, exchange rate (τ) and volume fraction (ρ). The range of each parameter is shown in Table 1. The objective function to be maximized is defined in terms of the inner product as:

$$C = \frac{\langle \hat{X}_{rs}, X_{rs} \rangle}{\|\hat{X}_{rs}\|_2 \|X_{rs}\|_2}. \quad (1)$$

The objective function measures the similarity as the cosine of the angle between the T-dimensional input signal X_{rs} and the guess $\hat{X}_{rs}$. We note that function evaluation in this task is computationally expensive. Since we cannot pregenerate the dictionary, each function call involves running a simulator to create the trajectory $\hat{X}_{rs}$ at a new guess of the

Algorithm 1 HybridSearch$\big(X^0, T_0, S, k^0, K, p, MaxIter\big)$

for $r = 1$ **to** R **{Iterating over row indices} do**
  for $s = 1$ **to** R **{Iterating over column indices} do**
    $i \leftarrow 0$
    while $i \leq MaxIter$ **do**
      $\{X^l_{rs}\}$ **= GenerateHypercube**$\big(X^i_{rs}, k^0, p\big)$
      if $random(0,1) < \gamma$ **then**
        $X^{i+1}_{rs} \leftarrow X^{\hat{l}}_{rs}$ **for** $\hat{l} = \underset{l}{argmax}\ \frac{\langle X^l_{rs}, S_{rs}\rangle}{\|X^l_{rs}\|_2 \|S_{rs}\|_2}$
      else
        $X^{i+1}_{rs} \leftarrow X^{\hat{l}}_{rs}$ **for** $\hat{l} = random(1, 2p)$
      $i \leftarrow i + 1$
    $\hat{X}_{rs}$ **= PatternSearch**$\big(X^i_{rs}, S_{rs}, k^0, \mathbf{K}, p, MaxIter\big)$
Return $\hat{X}$

Algorithm 2 GenerateHypercube (X, δ, d)

for $i = 1$ **to** d **do**
  $X_{new}[i] \leftarrow X[i] + \delta$
  $X_{new}[2i] \leftarrow X[i] - \delta$
Return $\{X^i_{new}\} \forall i \in (1, \ldots, 2d)$

six tissue properties. Each signal is generated using Monte Carlo simulations of 200 protons and subjected to the same MRF-X pulse sequence used in the scanner. For each combination of tissue properties, a unique signal is generated which is then used in the objective function. This is an unavoidable space-time tradeoff. However, because the search space is very large and very noisy, it is important to initialize the search from a reasonable starting point. To do this we use a small fixed dictionary of 10000 elements, uniformly distributed across the search space. Given a new trajectory, we find the closest match in this initialization dictionary using the objective function. We denote this initial guess as X^0_{rs}.

Tissue property	Minimum value	Maximum value	Step Size
$T1a(ms)$	100	1200	10
$T2a(ms)$	20	120	5
$T1b(ms)$	1200	3000	10
$T2b(ms)$	120	300	5
$log_{10}(\tau(s^{-1}))$	-2	0	-1
$log_{10}(\tau(s^{-1}))$	0	1	0.6
$log_{10}(\tau(s^{-1}))$	1	2	0.6
$\rho(\%)$	1	99	2

Table 1: Tissue property value bounds for the search space.

The approach we use is shown in Algorithm 1. This takes as input an initial guess X^0, signal $S \in R \times S \times T$, Temperature parameter T_0, and maximum iterations $MaxIter$. It additionally, takes parameters K, k^0, and p, which represent the maximum search distance, initial mesh size and number of tissue parameters, respectively. For each pixel in the input image, we perform two searches in succession. The first is Simulated Annealing. Simulated annealing (SA) is

Algorithm 3 PatternSearch$\big(X^0, S, k^0, K, p, MaxIter\big)$

for $r = 1$ **to** R **{Iterating over row indices} do**
  for $s = 1$ **to** R **{Iterating over column indices} do**
    $i \leftarrow 0; k \leftarrow k^0$
    while $k \leq K$ **and** $i \leq MaxIter$ **do**
      $\{X^l_{rs}\}$ **= GenerateHypercube**$\big(X^i_{rs}, k, p\big)$
      $C1 \leftarrow \frac{\langle X^l_{rs}, S_{rs}\rangle}{\|X^l_{rs}\|_2 \|S_{rs}\|_2} \geq \frac{\langle X^i_{rs}, S_{rs}\rangle}{\|X^i_{rs}\|_2 \|S_{rs}\|_2}\ \ l \in (1, 2p)$
      $C2 \leftarrow \frac{\langle X^l_{rs}, S_{rs}\rangle}{\|X^l_{rs}\|_2 \|S_{rs}\|_2} \leq \frac{\langle X^i_{rs}, S_{rs}\rangle}{\|X^i_{rs}\|_2 \|S_{rs}\|_2}\ \ \forall\, l \in (1, 2p)$
      if $C1$ **then**
        $k \leftarrow 2k$
        $X^{i+1}_{rs} \leftarrow X^{\hat{l}}_{rs}$ **for** $\hat{l} = \underset{l}{argmax}\ \frac{\langle X^l_{rs}, S_{rs}\rangle}{\|X^l_{rs}\|_2 \|S_{rs}\|_2}$
      else if $C2$ **then**
        $k \leftarrow \frac{k}{2}$
        $X^{i+1}_{rs} \leftarrow X^i_{rs}$
      $i \leftarrow i + 1$
    $\hat{X}_{rs} \leftarrow X^i_{rs}$
Return $\hat{X}$

a stochastic search technique that is effective at searching large, noisy search spaces. During this phase, we use simulated annealing with an acceptance function defined as

$$\gamma = \frac{1}{1 + exp\left(\frac{\Delta}{max(T_0)}\right)} \tag{2}$$

where γ is the probability of acceptance, Δ is the difference between function value at new point and old point, and T_0 is the temperature of simulated annealing. Using a step size as shown in Table 1, a set of neighbors to the current guess is chosen by the **GenerateHypercube** function (Algorithm 2) by taking a step with each parameter value. We evaluate the objective function at each of the neighbors and choose to move in the direction increasing functional value with probability γ, or randomly with probability $1 - \gamma$. Simulated annealing terminates when it reaches a predefined number of function evaluations. When it terminates, the point obtained may still not be a (local) maximum of the objective function because of the stochastic nature of the algorithm. At this point, we use a second, deterministic search called pattern search which refines the solution found by simulated annealing.

Generalized pattern search (Audet and Dennis Jr 2002) is a derivative-free greedy search with adjustable length scales to find an optimum solution. The goal of such a method is to avoid explicit calculation of gradient on the noisy high dimensional error surface.

We provide the pseudo-code of the pattern search algorithm (Algorithm 3). The algorithm iterates over each pixel of the MRF-X image to generate the tissue property maps. We initialize the algorithm with the best guess from the simulated annealing search. The pattern search algorithm also takes as input K, $MaxIter$, and p, which represent the maximum search distance, maximum iterations and number of parameters, respectively. We use a length parameter k^0 that

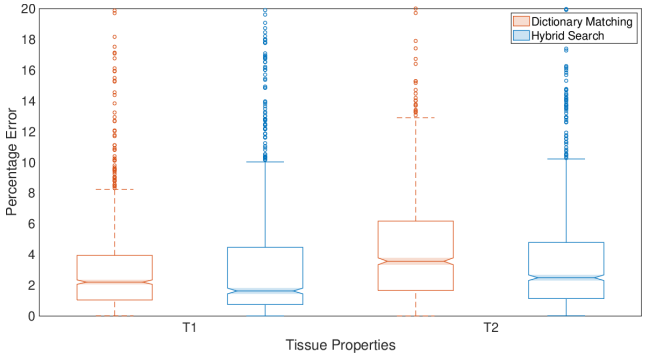

Figure 4: Box and Whisker plot of tissue property values T1 and T2, comparing Hybrid Search with dictionary matching ("Direct match"). The plots represent the mean squared error.

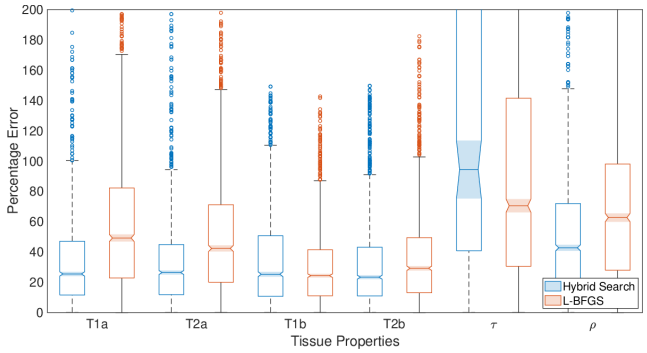

Figure 5: Box and Whisker plot of tissue property values T1a, T2a, T1b, T2b, τ, ρ, comparing Hybrid Search and L-BFGS. The plots represent the mean squared error.

is initialized to a preset length at the start of the iteration. As before, **GenerateHypercube** generates the neighbors of the current point, which are on the edge of the hypercube centered around the current guess. The algorithm accepts a new point if the function value is larger than the current guess. The current guess is now shifted to the new point, and the procedure repeated. If the current guess is larger than all the neighbors, we choose the point with the largest function value and cut the length parameter by half. Conversely if the current guess is smaller than all the neighbors, the length parameter is doubled. When the algorithm exceeds the maximum iterations or maximum search distance, the algorithm exits and returns the best guess $\hat{X}$. This is then returned as the found solution by the Hybrid Search procedure.

Results and Discussion

Our primary hypothesis is that using our Hybrid Search approach, we will be able to tractably extract locally optimal values for six tissue properties from each pixel of MRF images, something which is impossible with the current state of the art. First, we validate the performance of our approach when just recovering two tissue properties, T1 and T2, from MRF data. In this case we can also use the dictionary matching procedure, which is the state of the art. We generated data for 5000 (T1, T2) targets using pulse sequences similar to previous work (Ma et al. 2013). White Gaussian noise with SNR 5.0 was added to simulate realistic signals captured at the scanner. Each method produces estimated (T1, T2) values and we then compute the normalized root mean squared error for each property. The results are shown in Figure 4.

From the figure, we observe that both approaches produce excellent results in this case, typically within $2-4\%$ of the target values. This is expected for dictionary matching, and shows that our approach can provide similar results. Perhaps surprisingly, our approach slightly (though not significantly) outperforms the dictionary matching procedure on average by about 1%. This may be because a step size is necessary to generate a dictionary. We used a step size of $5ms$ in T1 and $3ms$ in T2. However, in the pattern search procedure, it is possible to search at a finer granularity and find more accurate matches.

We next evaluate our approach with the task of recovering six tissue properties T1a, T2a, T1b, T2b, τ, and ρ. We again generated 50000 targets with values for the six tissue properties uniformly distributed across the entire search space, and used MRF-X pulse sequence parameters used in (Hamilton, Griswold, and Seiberlich 2015). Because of this distribution of targets, we are evaluating the approach in regions where the MRF-X sequence has high sensitivity as well as low sensitivity. This range covers the values that were observed in normal white matter, grey matter, and abnormalities, such as meningioma. White Gaussian noise with SNR 5.0 was added to simulate realistic signals captured at the scanner. We provide a baseline using L-BFGS (Fletcher 1987). This is a deterministic gradient-based quasi-Newton optimization method. In this case, since the gradient is not computable in closed form, we use numerical gradient estimation at each candidate point to perform the search. We also provide summary statistics for mean and median absolute error over all six properties (T1a, T2a, T1b, T2b, τ, and ρ) in Table 2 for "idealized" dictionary matching, L-BFGS and Hybrid Search. In this case, true dictionary matching is impossible. However, we create an "idealized" comparison by creating a hypercube centered around each target point with the distance from center in each direction, T1a=300ms, T2a=20ms, T1b=300ms, T2b=20ms, τ=0.3s^{-1}, ρ=6. Then we generate the dictionary within this hypercube and perform matching with it. Obviously, in real scenarios, the true targets are unknown, so this approach cannot be used. However, it gives us an "ideal" lower bound of how well it is possible to do if the initial point of the optimizer lies in this hypercube. The results are shown in Figure 5 and Table 2.

From the figure, we first observe that the errors in recovering the target values are significantly higher in the 6D case than in the 2D case. This is because of two reasons: first, the noisiness of the MRF signal means that the search space is significantly non-smooth. Relatively close tissue properties can have very different objective function values, which is challenging to handle. Second, while we are using a

Algorithms	Dictionary Matching		L-BFGS		Hybrid Search	
Tissue Properties	Me	Md	Me	Md	Me	Md
T1a	0.13	0.11	0.39	0.37	0.24	0.25
T2a	0.18	0.12	0.52	0.39	0.36	0.36
T1b	0.07	0.07	0.31	0.25	0.24	0.25
T2b	0.16	0.15	0.48	0.35	0.27	0.25
τ	0.07	0.02	3.96	0.61	2.75	0.68
ρ	0.3	0.14	1.8	0.59	1.95	0.37

Table 2: Mean (Me) and median (Md) absolute error over six tissue properties for dictionary matching, L-BFGS, and Hybrid Search.

fixed pulse sequence, the targets are widely distributed. This means that the pulse sequence may not be sensitive to many targets, increasing the error. From the component-wise error, we observe that some of the tissue properties are estimated better than others. For example, T1a, T1b, T2a and T2b are relatively more accurate than τ and ρ. This likely means that the objective function was more sensitive to the last two values than the first four. Finally, we observe that the gradient-based baseline, L-BFGS, generally returned solutions that were less accurate than our approach. Again, this indicates a noisy non-smooth search space where deterministic gradient search can easily be trapped in local optima.

From the table, we observe that the "ideal" dictionary match has better mean and median absolute error than L-BFGS and Hybrid Search. This is expected, since it is doing an exhaustive search in a small, correct neighborhood of the target. Along some axes, such as T1a and T2b, Hybrid Search is only $\sim 10\%$ worse than an exhaustive match even though it generally does not start so close to the target as the "ideal" match, which is very promising. Along other axes such as τ, there may be room for improvement. While there remain opportunities for improvement, our approach is still able to solve these problems and recover six tissue properties tractably, which is an advance over the state of the art.

Path to Deployment

Challenges remain to be addressed on the path to deployment for MRF-X. As we see above, while our approach is tractable, its accuracy should be improved. Part of this must involve pulse sequence optimization, because if the sequence used is nowhere sensitive to the target properties, it is difficult for the search to recover the target. This is an iterative process, but the results can be applied at any stage to the clinical setting through computer-aided radiological diagnosis applications. These are already used by by radiologists to help diagnosis procedures. Figure 6 shows an example tool UI enhanced with the tissue properties we recover. We envision that our approach will allow a radiologist to select a region of interest from a standard T1w/T2w image where he or she suspects an abnormality. The tool will then reconstruct the other tissue properties of that region using our approach and display the tissue property maps of the selected region. This will allow for rapid diagnosis when radiologist believes there is a need for further investigation but conserves computational resources when there is certainty in negative diagnosis. Figure 6 shows a T1w image and a T2w image of a patient suffering from meningioma. When a radiologist selects a region of interest as shown in the image, we provide six tissue property maps of the region. The figure illustrates normal region tissue property values with T1a=465ms, T2a=26ms, T1b=1070ms, T2b=117ms, τ=7.14s^{-1}, ρ=30 and for abnormal region as T1a=375ms, T2a=20ms, T1b=1270ms, T2b=140ms, τ=0.6s^{-1}, ρ=25. These values were chosen due to their clinical significance with compartment A representing fat and compartment B representing non-fat tissue in white matter region of the brain (Deoni et al. 2008). We hypothesize that access to more tissue properties will increase diagnostic sensitivity and provide as yet unknown diagnostic opportunities for other diseases.

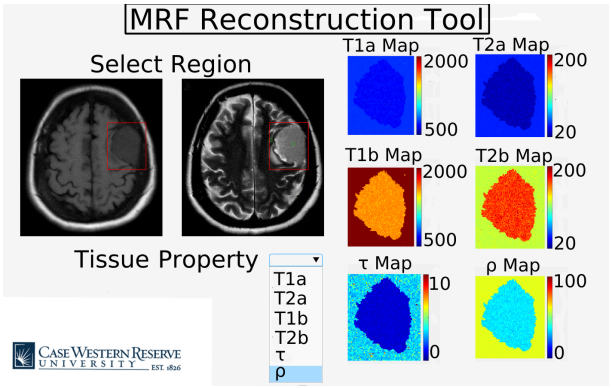

Figure 6: Proposed reconstruction tool for visualizing six tissue property maps from MRF scan. In the GUI, user selects a region that needs to be reconstructed. Selected tissue property maps are generated as shown in the GUI.

Conclusions

In our work, we have discussed an important emerging application, reconstructing multiple tissue properties using a single MRF scan. We introduce a hybrid search algorithm that uses a combination of stochastic and deterministic search strategies to enable recovery of 6 tissue properties that were intractable previously. A path to deployment of our method in the clinic is to extend computer-aided radiological diagnosis tools to show the reconstructed tissue property maps, improving diagnostic sensitivity and possibly enabling new diagnosis procedures.

Acknowledgments

We thank Dr. Nicole Seiberlich for providing direction, guidance and providing the simulation code that made this work possible. N. N. was partially supported by NSF CAREER award NSF-2002887. We also would like to thank High Performance Computing Center at CWRU for providing computing resources.

References

Audet, C.; and Dennis Jr, J. E. 2002. Analysis of generalized pattern searches. *SIAM Journal on optimization*, 13(3): 889–903.

Bernstein, M. A.; King, K. F.; and Zhou, X. J. 2004. *Handbook of MRI pulse sequences*. Elsevier.

Bloch, F. 1946. Nuclear Induction. *Phys. Rev.*, 70: 460–474.

Brown, R. W.; Cheng, Y.-C. N.; Haacke, E. M.; Thompson, M. R.; and Venkatesan, R. 2014. *Magnetic resonance imaging: physical principles and sequence design*. John Wiley & Sons.

Cauley, S. F.; Setsompop, K.; Ma, D.; Jiang, Y.; Ye, H.; Adalsteinsson, E.; Griswold, M. A.; and Wald, L. L. 2015. Fast group matching for MR fingerprinting reconstruction. *Magnetic Resonance in Medicine*, 74(2): 523–528.

Deoni, S. C.; Rutt, B. K.; Arun, T.; Pierpaoli, C.; and Jones, D. K. 2008. Gleaning multicomponent T1 and T2 information from steady-state imaging data. *Magnetic Resonance in Medicine*, 60(6): 1372–1387.

Deshmane, A.; McGivney, D. F.; Ma, D.; Jiang, Y.; Badve, C.; Gulani, V.; Seiberlich, N.; and Griswold, M. A. 2019. Partial volume mapping using magnetic resonance fingerprinting. *NMR in Biomedicine*, 32(5): e4082. E4082 NBM-18-0120.R2.

Fletcher, R. 1987. *Practical Methods of Optimization (2nd ed.)*. John Wiley & Sons.

Ginat, D. T.; and Meyers, S. P. 2012. Intracranial Lesions with High Signal Intensity on T1-weighted MR Images: Differential Diagnosis. *RadioGraphics*, 32(2): 499–516. PMID: 22411945.

Hamilton, J. I.; Griswold, M. A.; and Seiberlich, N. 2015. MR Fingerprinting with chemical exchange (MRF-X) to quantify subvoxel T1 and extracellular volume fraction. *Journal of Cardiovascular Magnetic Resonance*, 17(1): 1–3.

Jack, C. R.; Bernstein, M. A.; Fox, N. C.; Thompson, P.; Alexander, G.; Harvey, D.; Borowski, B.; Britson, P. J.; Whitwell, J. L.; Ward, C.; Dale, A. M.; Felmlee, J. P.; Gunter, J. L.; Hill, D. L.; Killiany, R.; Schuff, N.; Fox-Bosetti, S.; Lin, C.; Studholme, C.; DeCarli, C. S.; Krueger, G.; Ward, H. A.; Metzger, G. J.; Scott, K. T.; Mallozzi, R.; Blezek, D.; Levy, J.; Debbins, J. P.; Fleisher, A. S.; Albert, M.; Green, R.; Bartzokis, G.; Glover, G.; Mugler, J.; and Weiner, M. W. 2008. The Alzheimer's Disease Neuroimaging Initiative (ADNI): MRI methods. *Journal of Magnetic Resonance Imaging*, 27(4): 685–691.

Jiang, Y.; Ma, D.; Keenan, K. E.; Stupic, K. F.; Gulani, V.; and Griswold, M. A. 2017. Repeatability of magnetic resonance fingerprinting T1 and T2 estimates assessed using the ISMRM/NIST MRI system phantom. *Magnetic resonance in medicine*, 78(4): 1452–1457.

Kim, R. J.; Wu, E.; Rafael, A.; Chen, E. L.; Parker, M. A.; Simonetti, O.; Klocke, F. J.; Bonow, R. O.; and Judd, R. M. 2000. The use of contrast-enhanced magnetic resonance imaging to identify reversible myocardial dysfunction. *The New England Journal of Medicine*, 343(20): 1445–1453.

Körzdörfer, G.; Pfeuffer, J.; Kluge, T.; Gebhardt, M.; Hensel, B.; Meyer, C. H.; and Nittka, M. 2019. Effect of spiral undersampling patterns on FISP MRF parameter maps. *Magnetic Resonance Imaging*, 62: 174–180.

Larsson, H. B. W.; Frederiksen, J.; Petersen, J.; Nordenbo, A.; Zeeberg, I.; Henriksen, O.; and Olesen, J. 1989. Assessment of demyelination, edema, and gliosis by in vivo determination of T1 and T2 in the brain of patients with acute attack of multiple sclerosis. *Magnetic Resonance in Medicine*, 11(3): 337–348.

Ma, D.; Gulani, V.; Seiberlich, N.; Liu, K.; Sunshine, J. L.; Duerk, J. L.; and Griswold, M. A. 2013. Magnetic resonance fingerprinting. *Nature*, 495(7440): 187–192.

McGivney, D. F.; Pierre, E.; Ma, D.; Jiang, Y.; Saybasili, H.; Gulani, V.; and Griswold, M. A. 2014. SVD Compression for Magnetic Resonance Fingerprinting in the Time Domain. *IEEE Transactions on Medical Imaging*, 33(12): 2311–2322.

Wang, C. Y.; Coppo, S.; Mehta, B. B.; Seiberlich, N.; Yu, X.; and Griswold, M. A. 2019. Magnetic resonance fingerprinting with quadratic RF phase for measurement of T2* simultaneously with δf, T1, and T2. *Magnetic Resonance in Medicine*, 81(3): 1849–1862.

Yang, M.; Ma, D.; Jiang, Y.; Hamilton, J.; Seiberlich, N.; Griswold, M. A.; and McGivney, D. 2018. Low rank approximation methods for MR fingerprinting with large scale dictionaries. *Magnetic Resonance in Medicine*, 79(4): 2392–2400.

Yao, A.; Pain, M.; Balchandani, P.; and Shrivastava, R. K. 2018. Can MRI predict meningioma consistency?: a correlation with tumor pathology and systematic review. *Neurosurgical review*, 41(3): 745–753.